

Wave Effects in Gravitational Lensing of Gravitational Waves from Chirping Binaries

Ryuichi Takahashi and Takashi Nakamura

Department of Physics, Kyoto University, Kyoto 606-8502, Japan

ABSTRACT

In the gravitational lensing of gravitational waves, the wave optics should be used instead of the geometrical optics when the wavelength λ of the gravitational waves is longer than the Schwarzschild radius of the lens mass M_L . For the gravitational lensing of the chirp signals from the coalescence of the super massive black holes at the redshift $z_S \sim 1$ relevant to LISA, the wave effects become important for the lens mass smaller than $\sim 10^8 M_\odot$. For such cases, we compute how accurately we can extract the mass of the lens and the source position from the lensed signal. We consider two simple lens models: the point mass lens and the SIS (Singular Isothermal Sphere). We find that the lens mass and the source position can be determined within $\sim 0.1\% [(S/N)/10^3]^{-1}$ for the lens mass larger than $10^8 M_\odot$ and $\gtrsim 10\% [(S/N)/10^3]^{-1}$ for the lens mass smaller than $10^7 M_\odot$ due to the diffraction effect, where (S/N) is the signal to noise ratio of the unlensed chirp signals. For the SIS model, if the source position is outside the Einstein radius, only a single image exists in the geometrical optics approximation so that the lens parameters can not be determined. While in the wave optics cases we find that the lens mass can be determined even for $M_L < 10^8 M_\odot$. For the point mass lens, one can extract the lens parameters even if the source position is far outside the Einstein radius. As a result, the lensing cross section is an order of magnitude larger than that for the usual strong lensing of light.

Subject headings: gravitational lensing – gravitational waves – binaries

1. Introduction

Inspirals and mergers of compact binaries are the most promising gravitational wave sources and will be detected by the ground based as well as the space based detectors in the near future (e.g. Cutler & Thorne 2002). Laser interferometers are now coming on-line or planned on broad frequency bands: for the high frequency band $10-10^4$ Hz, the ground based

interferometers such as TAMA300, LIGO, VIRGO and GEO600 will be operated; for the low frequency band $10^{-4} - 10^{-1}$ Hz, the Laser Interferometer Space Antenna¹ (LISA) will be in operation; for the intermediate frequency band $10^{-2} - 1$ Hz, the space based interferometers such as DECIGO (Seto, Kawamura & Nakamura 2001) are planned. For the templates of the chirp signals from coalescing compact binaries, the post-Newtonian computations of the waveforms have been done by many authors. Using the matched filter techniques with the template, we can obtain the binary parameters such as the mass and the spatial position of the source (e.g. Cutler & Flanagan 1994).

If the gravitational waves from coalescing binary pass near massive objects, gravitational lensing should occur in the same way as it does for light. The gravitational lensing of light is usually treated in the geometrical optics approximation, which is valid in all the observational situations (Schneider, Ehlers & Falco 1992; Nakamura & Deguchi 1999). However for the gravitational lensing of gravitational waves, the wavelength is long so that the geometrical optics approximation is not valid in some cases. For example, the wavelength λ of the gravitational waves for the space interferometer is ~ 1 AU which is extremely larger than that of a visible light ($\lambda \sim 1\mu$ m). As shown by several authors (Ohanian 1974, Bliokh & Minakov 1975, Bontz & Haugan 1981, Thorne 1983, Deguchi & Watson 1986a), if the wavelength λ is larger than the Schwarzschild radius of the lens mass M_L , the diffraction effect is important and the magnification is small. To see the reason why the ratio M_L/λ determines the significance of the diffraction, we consider a double slit with the slit width comparable to the Einstein radius $\xi_E \sim (M_L D)^{1/2}$ where D is the distance from the screen to the slit (Nakamura 1998). When waves with the wavelength λ pass through the slit, the interference pattern is produced on the screen. The width ℓ of the central peak of the interference pattern is $\ell \sim (D/\xi_E)\lambda$. Then the maximum magnification of the wave flux is of the order $\sim \xi_E/\ell \sim M_L/\lambda$. Thus the diffraction effect is important for

$$M_L \lesssim 10^8 M_\odot \left(\frac{f}{\text{mHz}} \right)^{-1}, \quad (1)$$

where f is the frequency of the gravitational waves. However as suggested by Ruffa (1999), the focused region by the gravitational lensing would have a relatively large area because of the diffraction, so that the lensing probability will increase. Since the gravitational waves from the compact binaries are coherent, the interference is also important (Mandzhos 1981, Ohanian 1983, Schneider & Schmid-Burgk 1985, Deguchi & Watson 1986b, Peterson & Falk 1991). Thus we expect that the wave effects (diffraction and interference) would provide much information about the lens objects.

¹See <http://lisa.jpl.nasa.gov/index.html>

In this paper, we consider the wave effects in the gravitational lensing of gravitational waves. We take the coalescence of the super massive black holes (SMBHs) of mass $10^4 - 10^7 M_\odot$ as the sources. SMBH binary is one of the most promising sources for LISA and will be detected with very high signal to noise ratio, $S/N \sim 10^3$ (Bender *et al.* 2000). Since the merging SMBHs events will be detected for extremely high redshift ($z > 5$), the lensing probability is relatively high and hence some lensing events are expected. We consider the two simple lens models; 1) the point mass lens in which compact objects (such as black holes) are assumed as lens objects and 2) the SIS (Singular Isothermal Sphere) lens in which galaxies, star clusters and CDM (Cold Dark Matter) halos are assumed as lens. The wave effects become important for the lens mass $10^6 - 10^9 M_\odot$ which is determined by the LISA band, 10^{-4} to 10^{-1} Hz from Eq.(1). The frequency of the gravitational waves from the coalescing SMBH binary chirps so that we could see wave effects for different frequency in the lensed chirp signals.

We calculate the gravitational lensed waveform using the wave optics for the two lens models: the point mass lens and the SIS. Then, we investigate how accurately we can extract the information on the lens object from the gravitational lensed signals detected by LISA using the Fisher-matrix formalism (e.g. Cutler & Flanagan 1994). Cutler (1998) studied the estimation errors for the merging SMBHs by LISA (see also Vecchio & Cutler 1998; Hughes 2002; Moore & Hellings 2002; Hellings & Moore 2002; Seto 2002; Vecchio 2003). Following Cutler (1998), we calculate the estimation errors, especially for the lens mass and the source position. We assume the 1 yr observation before the final merging and consider the lens mass in the range $10^6 - 10^9 M_\odot$. Then the typical time delay between the double images is $10 - 10^4$ sec which is much smaller than 1 yr.

This paper is organized as follows. In §2, we briefly review the wave optics in gravitational lensing for the point mass lens and the SIS model. In §3, we discuss the gravitational lensed waveforms detected with LISA, and mention the parameter estimation based on the matched filtering analysis. In §4, we numerically evaluate the signal to noise ratio and the parameter estimation errors. We discuss the dependence of the estimation errors on the lens model, the lens mass and the source position. In §5, we estimate the lensing event rate. §6 is devoted to summary and discussions. We assume the $(\Omega_M, \Omega_\Lambda) = (0.3, 0.7)$ cosmology and the Hubble parameter $H_0 = 70$ km/sec/Mpc, and use the units of $c = G = 1$.

2. Wave Optics in Gravitational Lensing

In this section, we briefly review the wave optics in the gravitational lensing of the gravitational waves (Schneider, Ehlers & Falco 1992; Nakamura & Deguchi 1999). We consider

the gravitational waves propagating under the gravitational potential of the lens object. The metric is given by

$$ds^2 = -(1 + 2U) dt^2 + (1 - 2U) d\mathbf{r}^2 \equiv g_{\mu\nu}^{(B)} dx^\mu dx^\nu, \quad (2)$$

where $U(\mathbf{r})$ ($\ll 1$) is the gravitational potential of the lens object. Let us consider the linear perturbation $h_{\mu\nu}$ in the background metric tensor $g_{\mu\nu}^{(B)}$ as

$$g_{\mu\nu} = g_{\mu\nu}^{(B)} + h_{\mu\nu}. \quad (3)$$

Under the transverse traceless Lorentz gauge condition of $h^\nu{}_{\mu;\nu} = 0$ and $h^\mu{}_\mu = 0$ we have

$$h_{\mu\nu;\alpha}{}^{;\alpha} + 2R_{\alpha\mu\beta\nu}^{(B)} h^{\alpha\beta} = 0, \quad (4)$$

where $;$ is the covariant derivative with respect to $g_{\mu\nu}^{(B)}$ and $R_{\alpha\mu\beta\nu}^{(B)}$ is the background Riemann tensor. If the wavelength λ is much smaller than the typical radius of the curvature of the background, we have

$$h_{\mu\nu;\alpha}{}^{;\alpha} = 0. \quad (5)$$

Following the eikonal approximation to the above equation by Baraldo, Hosoya and Nakamura (1999), we express the gravitational wave as

$$h_{\mu\nu} = \phi e_{\mu\nu}, \quad (6)$$

where $e_{\mu\nu}$ is the polarization tensor of the gravitational wave ($e^\mu{}_\mu = 0$, $e_{\mu\nu}e^{\mu\nu} = 2$) and ϕ is a scalar. The polarization tensor $e_{\mu\nu}$ is parallelly transported along the null geodesic ($e_{\mu\nu;\alpha}k^\alpha = 0$, where k^α is a wave vector) (Misner, Thorne & Wheeler 1973). Then the change of the polarization tensor by gravitational lensing is of the order of U ($\ll 1$) which is very small in our observational situation, and hence we can regard the polarization tensor as a constant. Thus, we treat the scalar wave ϕ , instead of the gravitational wave $h_{\mu\nu}$, propagating through the curved space-time. The propagation equation of the scalar wave is

$$\partial_\mu(\sqrt{-g^{(B)}}g^{(B)\mu\nu}\partial_\nu\phi) = 0. \quad (7)$$

For the scalar wave in the frequency domain $\tilde{\phi}(f, \mathbf{r})$, the above equation (7) with Eq.(2) is rewritten as,

$$(\nabla^2 + \omega^2)\tilde{\phi} = 4\omega^2 U\tilde{\phi}, \quad (8)$$

where $\omega = 2\pi f$. The above equation (8) can be solved by using the Kirchhoff integral theorem (Schneider, Ehlers & Falco 1992).

It is convenient to define the amplification factor as

$$F(f) = \tilde{\phi}^L(f)/\tilde{\phi}(f), \quad (9)$$

where $\tilde{\phi}^L(f)$ and $\tilde{\phi}(f)$ are the lensed and unlensed ($U = 0$ in Eq.(8)) gravitational wave amplitudes, respectively. In Fig.1, we show the gravitational lens geometry of the source, the lens and the observer. D_L, D_S and D_{LS} are the distances to the lens, the source and from the source to the lens, respectively. $\boldsymbol{\eta}$ is a position vector of the source in the source plane while $\boldsymbol{\xi}$ is the impact parameter in the lens plane. We use the thin lens approximation in which the lens is characterized by the surface mass density $\Sigma(\boldsymbol{\xi})$ and the gravitational waves are scattered on the thin lens plane. Then, the amplification factor $F(f)$ at the observer is given by (Schneider, Ehlers & Falco 1992),

$$F(f) = \frac{D_S \xi_0^2}{D_L D_{LS}} \frac{f}{i} \int d^2\mathbf{x} \exp [2\pi i f t_d(\mathbf{x}, \mathbf{y})], \quad (10)$$

where $\mathbf{x} = \boldsymbol{\xi}/\xi_0$, and $\mathbf{y} = \boldsymbol{\eta} D_L / \xi_0 D_S$ is the source position. ξ_0 is the arbitrary normalization constant of the length. t_d is the arrival time at the observer from the source. F is normalized such that $|F| = 1$ in no lens limit ($U = 0$).

Though we do not take account of the cosmological expansion in the metric, Eq.(2), we can apply the result without the cosmological expansion to cosmological situations since the wavelength of the gravitational waves is much smaller than the horizon scale. What we should do is 1) take the angular diameter distances and 2) replace f with $f(1 + z_L)$ where z_L is the redshift of the lens (Baraldo, Hosoya and Nakamura 1999). Then the amplification factor $F(f)$ in Eq.(10) is rewritten in cosmological situations as,

$$F(f) = \frac{D_S \xi_0^2 (1 + z_L)}{D_L D_{LS}} \frac{f}{i} \int d^2\mathbf{x} \exp [2\pi i f t_d(\mathbf{x}, \mathbf{y})], \quad (11)$$

where D_L, D_S and D_{LS} denote the angular diameter distances. The arrival time t_d at the observer from the source position $\boldsymbol{\eta}$ through $\boldsymbol{\xi}$ is given by (Schneider, Ehlers & Falco 1992),

$$t_d(\mathbf{x}, \mathbf{y}) = \frac{D_S \xi_0^2}{D_L D_{LS}} (1 + z_L) \left[\frac{1}{2} |\mathbf{x} - \mathbf{y}|^2 - \psi(\mathbf{x}) + \phi_m(\mathbf{y}) \right], \quad (12)$$

The nondimensional deflection potential $\psi(\mathbf{x})$ is determined by

$$\nabla_x^2 \psi = 2\Sigma / \Sigma_{cr}, \quad (13)$$

where ∇_x^2 denotes the two-dimensional Laplacian with respect to \mathbf{x} , Σ is the surface mass density of the lens and $\Sigma_{cr} = D_S / (4\pi D_L D_{LS})$. We choose $\phi_m(\mathbf{y})$ so that the minimum value of the arrival time is zero. We derive $\psi(\mathbf{x})$ and $\phi_m(\mathbf{y})$ in the following subsections for the point mass lens and the SIS model.

In the geometrical optics limit ($f \gg t_d^{-1}$), the stationary points of the $t_d(\mathbf{x}, \mathbf{y})$ contribute to the integral of Eq.(11) so that the image positions \mathbf{x}_j are determined by the lens equation

$$\partial t_d(\mathbf{x}, \mathbf{y}) / \partial \mathbf{x} = 0. \quad (14)$$

This is just the Fermat's principle. The integral on the lens plane (in Eq.(11)) is reduced to the sum over these images (Nakamura & Deguchi 1999) as

$$F(f) = \sum_j |\mu_j|^{1/2} \exp [2\pi i f t_{d,j} - i\pi n_j], \quad (15)$$

where the magnification of the j -th image is $\mu_j = 1/\det(\partial\mathbf{y}/\partial\mathbf{x}_j)$, $t_{d,j} = t_d(\mathbf{x}_j, \mathbf{y})$ and $n_j = 0, 1/2, 1$ when \mathbf{x}_j is a minimum, saddle, maximum point of $t_d(\mathbf{x}, \mathbf{y})$. In the time domain the wave is expressed as

$$\phi^L(t, \mathbf{r}) = \sum_j |\mu_j|^{1/2} \phi(t - t_{d,j}, \mathbf{r}) \exp [-i\pi n_j]. \quad (16)$$

This shows that the oscillatory behavior of $F(f)$ in high frequency f is essential to obtain the time delay among the images.

2.1. Point Mass Lens

The surface mass density is expressed as $\Sigma(\boldsymbol{\xi}) = M_L \delta^2(\boldsymbol{\xi})$ where M_L is the lens mass. As the normalization constant ξ_0 we adopt the Einstein radius given by $\xi_0 = (4M_L D_L D_{LS}/D_S)^{1/2}$ while the nondimensional deflection potential is $\psi(\mathbf{x}) = \ln x$. In this case, Eq.(11) is analytically integrated as (Peters 1974),

$$F(f) = \exp \left[\frac{\pi w}{4} + i \frac{w}{2} \left(\ln \left(\frac{w}{2} \right) - 2\phi_m(y) \right) \right] \\ \times \Gamma \left(1 - \frac{i}{2} w \right) {}_1F_1 \left(\frac{i}{2} w, 1; \frac{i}{2} w y^2 \right), \quad (17)$$

where $w = 8\pi M_{Lz} f$; $\phi_m(y) = (x_m - y)^2/2 - \ln x_m$ with $x_m = (y + \sqrt{y^2 + 4})/2$; $M_{Lz} = M_L(1 + z_L)$ is the redshifted lens mass and ${}_1F_1$ is the confluent hypergeometric function. Thus, the amplification factor $F(f)$ includes the two lens parameters; the redshifted lens mass M_{Lz} and the source position y . In the geometrical optics limit ($f \gg M_{Lz}^{-1}$) from Eq.(15) we have

$$F(f) = |\mu_+|^{1/2} - i |\mu_-|^{1/2} e^{2\pi i f \Delta t_d}, \quad (18)$$

where the magnification of each image is $\mu_{\pm} = 1/2 \pm (y^2 + 2)/(2y\sqrt{y^2 + 4})$ and the time delay between the double images is $\Delta t_d = 4M_{Lz} [y\sqrt{y^2 + 4}/2 + \ln((\sqrt{y^2 + 4} + y)/(\sqrt{y^2 + 4} - y))]$. The typical time delay is $\Delta t_d \sim 4M_{Lz} = 2 \times 10^3 \text{ sec } (M_{Lz}/10^8 M_{\odot})$.

2.2. Singular Isothermal Sphere

The surface density of the SIS (Singular Isothermal Sphere) is characterized by the velocity dispersion v as, $\Sigma(\boldsymbol{\xi}) = v^2/(2\xi)$. As the normalization constant we adopt the Einstein radius $\xi_0 = 4\pi v^2 D_L D_{LS}/D_S$ and the nondimensional deflection potential is $\psi(\mathbf{x}) = x$. In this case $F(f)$ in Eq.(11) is expressed as

$$F(f) = -iw e^{iwy^2/2} \int_0^\infty dx x J_0(wxy) \exp \left[iw \left(\frac{1}{2}x^2 - x + \phi_m(y) \right) \right], \quad (19)$$

where J_0 is the Bessel function of zeroth order; $\phi_m(y) = y + 1/2$ and $w = 8\pi M_{Lz} f$ where M_{Lz} is defined as the mass inside the Einstein radius given by $M_{Lz} = 4\pi^2 v^4 (1 + z_L) D_L D_{LS}/D_S$. Then, $F(f)$ depends on the two lens parameters M_{Lz} and y . We computed the above integral numerically for various parameters. In the geometrical optics limit ($f \gg M_{Lz}^{-1}$), F is given by,

$$\begin{aligned} F(f) &= |\mu_+|^{1/2} - i |\mu_-|^{1/2} e^{2\pi i f \Delta t_d} & \text{for } y \leq 1, \\ &= |\mu_+|^{1/2} & \text{for } y \geq 1, \end{aligned} \quad (20)$$

where $\mu_\pm = \pm 1 + 1/y$ and $\Delta t_d = 8M_{Lz} y$. If $y \leq 1$, double images are formed.

The wave effects in gravitational lensing of gravitational waves were discussed for the point mass lens (Nakamura 1998; Ruffa 1999; De Paolis *et al.* 2002; Zakharov & Baryshev 2002) and a Kerr BH (Baraldo, Hosoya & Nakamura 1999). However as far as we know the wave effects for the SIS (Singular Isothermal Sphere) model have not been discussed although the SIS model can be used for more realistic lens objects such as galaxies and star clusters.

2.3. The Amplification Factor

In Fig.2, we show the amplification factor $|F(f)|$ as a function of $w (= 8\pi M_{Lz} f)$ for the fixed source position $y = 0.1, 0.3, 1, 3$ for the point mass lens (left panel) and the SIS lens (right panel). For $w \lesssim 1$, the amplification is very small due to the diffraction effect (e.g., Bontz & Haugan 1980). Since in this case the wave length is so long that the wave does not feel the existence of the lens. For $w \gtrsim 1$, $|F(f)|$ asymptotically converges to the geometrical optics limit (Eq.(18) and (20));

$$|F(f)|^2 = |\mu_+| + |\mu_-| + 2 |\mu_+ \mu_-|^{1/2} \sin(2\pi f \Delta t_d), \quad (21)$$

where $\mu_- = 0$ for $y \geq 1$ in the SIS. The first and second terms in Eq.(21), $|\mu| = |\mu_+| + |\mu_-|$, represent the total magnification in the geometrical optics. The third term expresses the

interference between the double images. The oscillatory behavior (in Fig.2) is due to this interference. The amplitude and the period of this oscillation are approximately equal to $2|\mu_+\mu_-|^{1/2}$ and $2\pi f\Delta t_d$ in the third term of Eq.(21), respectively. As the source position y increases, the total magnification $|\mu|$ ($= |\mu_+| + |\mu_-|$) and the amplitude of the oscillation $2|\mu_+\mu_-|^{1/2}$ decrease. This is because each magnification $|\mu_{\pm}(y)|$ decreases as y increases. We note that even for $y \geq 1$ in SIS model ($y = 3$ in Fig.2) the damped oscillatory behavior appears, which looks like the time delay factor of $\sin(2\pi f\Delta t_d)$ although only a single image exists in the geometrical optics limit.

Fig.3 is the same as Fig.2, but we show the phase of the amplification factor $\theta_F(f) = -i \ln[F(f)/|F(f)|]$. The behavior is similar to that of the amplitude (in Fig.2), and the wave effects appear in the phase θ_F as well as the amplitude $|F|$. For $w \gtrsim 1$, $\theta_F(f)$ asymptotically converges to the geometrical optics limit (Eq.(18) and (20));

$$\theta_F(f) = \arctan \left[\frac{-|\mu_-|^{1/2} \cos(2\pi f\Delta t_d)}{|\mu_+|^{1/2} + |\mu_-|^{1/2} \sin(2\pi f\Delta t_d)} \right], \quad (22)$$

where $\mu_- = 0$ for $y \geq 1$ in the SIS. From the above equation (22), the phase θ_F oscillates between $-\arctan(|\mu_-/\mu_+|^{1/2})$ and $\arctan(|\mu_-/\mu_+|^{1/2})$ with the period of $2\pi f\Delta t_d$. As the source position y increases, the magnification ratio $|\mu_-/\mu_+|$ and the amplitude of the oscillation $\arctan(|\mu_-/\mu_+|^{1/2})$ decrease.

3. Gravitational Lensed Waveform and Parameter Estimation

3.1. Gravitational Wave Measurement with LISA

We briefly discuss the gravitational wave measurement with LISA (see Cutler 1998; Bender *et al.* 2000). LISA consists of three spacecrafts forming an equilateral triangle and orbits around the Sun, trailing 20° behind the Earth. The sides of the triangle are $L = 5 \times 10^6$ km in length, and the plane of the triangle is inclined at 60° with respect to the ecliptic. The triangle rotates annually. The gravitational wave signal is reconstructed from the three data streams that effectively correspond to three time-varying armlength data. Two of the three data are linearly independent of each other. The data contain both gravitational waves signals to be fitted by matched filtering and noises which are assumed to be stationary, Gaussian and uncorrelated with each other (Cutler 1998). The gravitational wave signals $h_{I,II}(t)$ from a binary are written as

$$h_{I,II}(t) = \frac{\sqrt{3}}{2} [F_{I,II}^+(t)h_+(t) + F_{I,II}^\times(t)h_\times(t)], \quad (23)$$

where $F_{I,II}^{+,\times}(t)$ are the pattern functions which depend on the source's angular position of the binary, its orientation and detector's configuration. The quantities $h_{+,\times}(t)$ are the two polarization modes of gravitational radiation from the binary. The direction and the orientation of the binary and the direction of the lens are assumed to be constant during the observation in a fixed barycenter frame of the solar system. Further discussion and details about the pattern functions are shown in Cutler (1998).

3.2. Gravitational Lensed Signal Measured by LISA

We consider the SMBH binaries at redshift z_S as the sources. We use restricted post-Newtonian approximation as the in-spiral waveform (Cutler & Flanagan 1994). The coalescing time for circular orbit is typically $t_c = 0.1\text{yr} (\mathcal{M}_z/10^6 M_\odot)^{-5/3} (f/10^{-4}\text{Hz})^{-8/3}$ where $\mathcal{M}_z = (M_1 M_2)^{3/5} (M_1 + M_2)^{-1/5} (1 + z_S)$ is the redshifted chirp mass. At the solar system barycenter, the unlensed waveforms $\tilde{h}_{+,\times}(f)$ in the frequency domain are given by

$$\begin{aligned}\tilde{h}_+(f) &= \mathcal{A} [1 + (\mathbf{L} \cdot \mathbf{n})^2] f^{-7/6} e^{i\Psi(f)}, \\ \tilde{h}_\times(f) &= -2i\mathcal{A} (\mathbf{L} \cdot \mathbf{n}) f^{-7/6} e^{i\Psi(f)},\end{aligned}\tag{24}$$

where \mathbf{L} (given by $\bar{\theta}_L, \bar{\phi}_L$) is the unit vector in the direction of the binary's orbital angular momentum and \mathbf{n} (given by $\bar{\theta}_S, \bar{\phi}_S$) is the unit vector toward the binary. These vectors are defined in a fixed barycenter frame of the solar system. The amplitude \mathcal{A} and the phase $\Psi(f)$ depend on six parameters; the redshifted chirp mass \mathcal{M}_z and reduced mass $\mu_z = M_1 M_2 (1 + z_S) / (M_1 + M_2)$; the spin-orbit coupling constant β ; a coalescence time t_c and phase ϕ_c ; the angular diameter distance to the source D_S . The amplitude is

$$\mathcal{A} = \sqrt{\frac{5}{96}} \frac{\pi^{-2/3} \mathcal{M}_z^{5/6}}{D_S (1 + z_S)^2}.\tag{25}$$

where $D_S(1 + z_S)^2$ is the luminosity distance to the source, and $\Psi(f)$ is a rather complicated function of $\mathcal{M}_z, \mu_z, \beta, \phi_c$ and t_c (see Eq.(3.24) of Cutler & Flanagan 1994).

The gravitational lensed waveforms $\tilde{h}_{+,\times}^L(f)$ in the frequency domain are given by the product of the amplification factor $F(f)$ and the unlensed waveforms $\tilde{h}_{+,\times}(f)$ (see section 2);

$$\tilde{h}_{+,\times}^L(f) = F(f) \tilde{h}_{+,\times}(f).\tag{26}$$

where the function $F(f)$ is given in Eq.(11). Using Eq.(23),(24) and (26), the observed lensed signals $\tilde{h}_\alpha^L(f)$ ($\alpha = I, II$) with LISA are given in the stationary phase approximation as,

$$\tilde{h}_\alpha^L(f) = \frac{\sqrt{3} D_S \xi_0^2 (1 + z_L) f}{2 D_L D_{LS}} \int d^2\mathbf{x} \Lambda_\alpha(t + t_d(\mathbf{x}, \mathbf{y})) e^{2\pi i f t_d(\mathbf{x}, \mathbf{y})} e^{-i(\phi_D + \phi_{p,\alpha})(t + t_d(\mathbf{x}, \mathbf{y}))}$$

$$\times \mathcal{A}f^{-7/6}e^{i\Psi(f)}, \quad (27)$$

where $\phi_{p,\alpha}(t) = \tan^{-1}[2(\mathbf{L} \cdot \mathbf{n})F_\alpha^\times(t)/\{1 + (\mathbf{L} \cdot \mathbf{n})^2\}F_\alpha^+(t)]$ and $\Lambda_\alpha(t) = [(2\mathbf{L} \cdot \mathbf{n})^2F_\alpha^{\times 2}(t) + \{1 + (\mathbf{L} \cdot \mathbf{n})^2\}^2F_\alpha^{+ 2}(t)]^{1/2}$. The Doppler phase is $\phi_D(t) = 2\pi f(t)R \sin \bar{\theta}_S \cos(\bar{\phi}(t) - \bar{\phi}_S)$, $R = 1$ AU and $\bar{\phi}(t) = 2\pi t/T$ ($T = 1$ yr). $t = t(f)$ is given in Eq.(3.10) of Cutler & Flanagan (1994). In no lens limit of $\psi(\mathbf{x}) = 0$, the lensed signals $\tilde{h}_\alpha^L(f)$ in Eq.(27) agree with the unlensed ones $\tilde{h}_\alpha(f)$ in Cutler (1998). We assume the source position \mathbf{y} is constant during the observation, since the characteristic scale of the interference pattern, $\sim 10^7 \text{AU}(M_{Lz}/10^8 M_\odot)^{-1/2}(f/\text{mHz})^{-1} [(D_S D_L/D_{LS})/\text{Gpc}]^{1/2}$, is extremely larger than the LISA's orbital radius (1 AU).

Since the lensed signals $\tilde{h}_\alpha^L(f)$ in Eq.(27) are given by double integral, we approximate $\tilde{h}_\alpha^L(f)$ in the two limiting cases; 1) geometrical optics limit ($f \gg t_d^{-1}$) and 2) the time delay being much smaller than LISA's orbital period of ($t_d \ll 1$ yr). In the geometrical optics limit, from Eq.(15) we obtain,

$$\tilde{h}_\alpha^L(f) = \frac{\sqrt{3}}{2} \sum_j |\mu_j|^{1/2} \Lambda_\alpha(t + t_{d,j}) e^{2\pi i f t_{d,j} - i\pi n_j} e^{-i(\phi_D + \phi_{p,\alpha})(t + t_{d,j})} \times \mathcal{A}f^{-7/6}e^{i\Psi(f)}. \quad (28)$$

If the time delay is much smaller than LISA's orbital period ($t_d \ll 1$ yr), we expand Λ_α, ϕ_D and $\phi_{p,\alpha}$ around $t_d = 0$ as,

$$\begin{aligned} \tilde{h}_\alpha^L(f) &= \frac{\sqrt{3}}{2} \Lambda_\alpha(t) e^{-i(\phi_D + \phi_{p,\alpha})(t)} \times \mathcal{A}f^{-7/6}e^{i\Psi(f)} \\ &\times \left[F(f) + \frac{d}{dt} \{ \ln \Lambda_\alpha - i(\phi_D + \phi_{p,\alpha}) \} \frac{f}{2\pi i} \frac{d}{df} \left(\frac{F(f)}{f} \right) + \mathcal{O}((t_d/1\text{yr})^2) \right]. \end{aligned} \quad (29)$$

Since we consider the lens mass $M_{Lz} = 10^6 - 10^9 M_\odot$, the time delay is much smaller than 1 yr. Thus we use the above equation (29) as the lensed waveforms for the following calculations.

In Fig.4, the lensed signals $|\tilde{h}_\alpha^L(f)|$ ($\alpha = I, II$) and the unlensed ones $|\tilde{h}_\alpha(f)|$ are shown. We show the results from one year before the final merging to the inner most stable circular orbit (the binary separation is $r = 6(M_1 + M_2)$). We set typical parameters at the SMBH binary masses $M_{1,2z} = 10^6 M_\odot$, the lens mass $M_{Lz} = 10^8 M_\odot$ and the source position $y = 1$ for the point mass lens. The angular parameters are $\cos \bar{\theta}_S = 0.3, \bar{\phi}_S = 5.0, \cos \bar{\theta}_L = 0.8, \bar{\phi}_L = 2.0$, and the source redshift is $z_S = 1$ (the angular diameter distance is $H_0 D_S = 0.386$). Therefore the frequency range is from 5×10^{-5} to 2×10^{-3} Hz and the time delay is 4×10^3 sec. The strange behavior in the lower frequency $f \lesssim 10^{-4}$ Hz is due to the LISA's orbital motion. In this frequency region, however, the difference between the lensed signal and the unlensed one is small due to the diffraction (see Fig.2). On the other hand, the oscillatory behavior appears in the higher frequency region $f \gtrsim 10^{-4}$ Hz. This critical frequency is

determined by the inverse of the lens mass $8\pi M_{Lz}$ (see Fig.2). The oscillatory amplitude and the period are determined by the product of the magnifications $2|\mu_+\mu_-|^{1/2} = 2/(y\sqrt{y^2+4})$ and the inverse of the time delay, $1/\Delta t_d$ (see the third term of Eq.(21)).

3.3. Parameter Extraction

We briefly mention the matched filtering analysis and the parameter estimation errors (Finn 1992; Cutler & Flanagan 1994). We assume that the signal $\tilde{h}_\alpha^L(f)$ is characterized by some unknown parameters γ_i . In the present case, there are ten source parameters ($\mathcal{M}_z, \mu_z, \beta, \phi_c, t_c, D_S, \bar{\theta}_S, \bar{\phi}_S, \bar{\theta}_L, \bar{\phi}_L$) and two lens parameters (M_{Lz}, y). In the matched filtering analysis the variance-covariance matrix of the parameter estimation error $\Delta\gamma_i$ is given by inverse of the Fisher information matrix Γ_{ij} as $\langle\Delta\gamma_i\Delta\gamma_j\rangle = (\Gamma^{-1})_{ij}$. The Fisher matrix becomes

$$\Gamma_{ij} = 4 \sum_{\alpha=I,II} \text{Re} \int \frac{df}{Sn(f)} \frac{\partial \tilde{h}_\alpha^{L*}(f)}{\partial \gamma_i} \frac{\partial \tilde{h}_\alpha^L(f)}{\partial \gamma_j}, \quad (30)$$

where $Sn(f)$ is the noise spectrum. The noise spectrum $Sn(f)$ is the sum of the instrumental and the confusion noise, and we adopt the same noise spectrum as that in Cutler (1998). The signal to noise ratio (S/N) is given by

$$(S/N)^2 = 4 \sum_{\alpha=I,II} \int \frac{df}{Sn(f)} \left| \tilde{h}_\alpha^L(f) \right|^2. \quad (31)$$

We computed the variance-covariance matrix Γ_{ij} for a wide range of the lens parameters (M_{Lz}, y), using the lensed waveform in Eq.(29). Since the S/N is very high for the SMBH merger, the Fisher matrix approach to calculate the estimation errors is valid (Cutler 1998). We integrate gravitational lensed waveform (in Eq.(30) and Eq.(31)) from 1 yr before the final merging to the cut-off frequency f_{cut} when the binary separation becomes $r = 6(M_1 + M_2)$. We do not consider the low-frequency cut-off of LISA, which is low frequency noise wall of space-based instruments and is around $10^{-5} - 10^{-4}$ Hz (Vecchio 2003). This assumption is to underestimate the errors in estimation parameters.

4. Results

In this section, we present numerical results to compute the signal to noise ratio (S/N) and the errors in estimation parameters. We randomly distribute 100 binaries over various directions and orientations on celestial spheres at $z_S = 1$ (the distance is $H_0 D_S = 0.386$). We present the mean value averaged for 100 binaries.

4.1. Lensing Effects on the Signal to Noise Ratio

We demonstrate the gravitational lensing effect on the signal to noise ratio (S/N). In Fig.5, the increasing factor of S/N by the gravitational lensing for the point mass lens is shown for the fixed source position $y = 0.1, 0.3, 1, 3$ as a function of the lens mass M_{Lz} . The vertical axis is the S/N with the gravitational lensing divided by the unlensed S/N . Four panels are shown for the various SMBH binary masses $M_{1,2z} = 10^4, 10^5, 10^6, 10^7 M_\odot$. We show the mean value averaged for 100 binaries, but the dispersion is negligibly small (less than 5 %). For the lens mass smaller than $10^6 M_\odot$ the magnification is very small irrespective of the SMBH binary masses due to the diffraction effects. In this case the Schwarzschild radius of the lens mass M_{Lz} is smaller than the wavelength of gravitational waves $\lambda \sim 1$ AU, and the waves are not magnified by lensing. This critical lens mass ($10^6 M_\odot$) is mainly determined by the inverse of the knee frequency of the LISA's noise spectrum, $1/(8\pi f) \sim 8 \times 10^6 M_\odot (f/\text{mHz})^{-1}$ (see Fig.2). But for $10^7 + 10^7 M_\odot$, the SMBH binary coalescences at the lower frequency ($f \sim 10^{-4}$ Hz), thus the critical lens mass is shifted for larger mass ($10^7 M_\odot$) as shown in the right bottom panel of Fig.5. This tells us that if the lens mass is smaller than $10^6 M_\odot$, the effect of the lens is very small. If the lens mass is larger than $10^7 M_\odot$, the damped oscillatory behavior appears due to the interference between the two images, and the S/N converges to the geometrical optics limit, $|\mu|^{1/2} = (y^2 + 2)^{1/2}/[y^{1/2}(y^2 + 4)^{1/4}]$, which is independent of the lens mass. As y increases from 0.1 (solid line) to 3 (dashed line), the amplification decreases since the magnifications of the two images ($|\mu_\pm(y)|$) decrease as y increases (see also Fig.2).

Fig.6 is the same as Fig.5, but for the SIS lens model. The behavior is very similar to that in the point mass lens. For the lens mass larger than $10^7 M_\odot$, the S/N converges to the geometrical optics limit, $|\mu|^{1/2} = (2/y)^{1/2}$ for $y \leq 1$ and $|\mu|^{1/2} = (1 + 1/y)^{1/2}$ for $y \geq 1$. As y increases from 0.1 (solid line) to 3 (dashed line), the amplification decreases (see also the right panel of Fig.2).

4.2. Parameter Estimation for the Lens Objects

In this section, we show the parameter estimation for the lens objects. We show the results for the SMBH binary with masses $10^6 + 10^6 M_\odot$, because we found S/N is higher than the other binary masses ($M_{1,2z} = 10^4, 10^5$ and $10^7 M_\odot$). We distribute the 100 binaries over the various directions and the orientations at $z_S = 1$, and the mean value of the S/N without lensing is 2600 in these 100 binaries. We show the mean value of errors averaged for 100 binaries, for $M_{Lz} \lesssim 10^7 M_\odot$ the dispersion is relatively large ($\lesssim 40\%$), but for $M_{Lz} \gtrsim 10^7 M_\odot$ the results converge to that in the geometrical optics limit and the dispersion is negligibly

small.

In Fig.7, the estimation errors for the redshifted lens mass ΔM_{Lz} (left panel) and the source position Δy (right panel) are shown as a function of M_{Lz} with $y = 0.1, 0.3, 1, 3$ for the point mass lens. We use the units of $S/N = 10^3$, and the results (ΔM_{Lz} , Δy) scale as $(S/N)^{-1}$. For $M_{Lz} \lesssim 10^7 M_\odot$ the estimation errors are relatively large $\gtrsim 10\%$, since the effect of lensing on the signals is very small due to the diffraction. For $M_{Lz} \gtrsim 10^8 M_\odot$ the geometrical optics approximation is valid, and the errors converge to a constant in Fig.7. The redshifted lens mass and the source position can be determined up to the accuracy of $\sim 0.1\%$, as shown in Fig.7. The errors in the geometrical optics limit are well fitted by (see Appendix A),

$$\begin{aligned} \frac{\Delta M_{Lz}}{M_{Lz}} &= \frac{1}{S/N} \times \frac{\sqrt{y(y^2+2)}(y^2+4)^{5/4}}{2\tau}, \\ \frac{\Delta y}{y} &= \frac{1}{S/N} \times \frac{\sqrt{y^2+2}(y^2+4)^{3/4}}{2\sqrt{y}}, \end{aligned} \quad (32)$$

where S/N is in the unlensed case, and $\tau = \Delta t_d/4M_{Lz} = y\sqrt{y^2+4}/2 + \ln((\sqrt{y^2+4} + y)/(\sqrt{y^2+4} - y))$. Thus, one could determine the lens parameters, the redshifted lens mass and the source position, up to the accuracy of $\sim (S/N)^{-1}$. The above equations (32) are valid if the time delay Δt_d is much smaller than the LISA's orbital period 1 yr. If the time delay Δt_d becomes comparable to 1 yr, the LISA's orbital motion affects the results.

Fig.8 is the same as Fig.7, but as a function of y . For $y \gtrsim 1$, the errors are convergent to the geometrical optics limit of Eq.(32) irrespective of the lens mass. As y increases, the time delay t_d increases, and the geometrical optics limit ($ft_d \gg 1$) is valid. We note that even for $y \gtrsim 10$ one can extract the lens information. In the case of light, the observable is the lensed flux which is proportional to the magnifications, $\propto |\mu_\pm|$, but for gravitational waves the observable is the lensed amplitude which is proportional to the square root of the magnifications $\propto |\mu_\pm|^{1/2}$. For example, let us consider the case where the flux ratio of a brighter image to a fainter one is 100 : 1. Then the amplitude ratio is 10 : 1 so that the fainter image can be observed even if the source position is far from the Einstein radius in the case of gravitational waves. Denoting the largest source position for which one can extract the lens parameters as y_{cr} , we approximate the errors in Eq.(32) for the large y limit; $\Delta\gamma/\gamma \simeq (S/N)^{-1}y^2$, where $\gamma = M_{Lz}, y$. Then we obtain

$$y_{cr} \simeq 10 \left(\frac{\Delta\gamma/\gamma}{0.1} \right)^{1/2} \left(\frac{S/N}{10^3} \right)^{1/2}. \quad (33)$$

Thus the lensing cross section ($\propto y_{cr}^2$) increases an order of magnitude larger than that for the usual strong lensing of light ($y_{cr} = 1$) (e.g. Turner, Ostriker & Gott 1984).

In Fig.9, the estimation errors for the SIS model are shown. For $M_{Lz} \lesssim 10^7 M_\odot$ the behavior is similar for the point mass lens. But for $M_{Lz} \gtrsim 10^8 M_\odot$ the behavior strongly depends on y . In the geometrical optics approximation, the errors are given by (Appendix A),

$$\frac{\Delta M_{Lz}}{M_{Lz}} = \frac{\Delta y}{y} = \frac{1}{S/N} \times \sqrt{\frac{2(1-y^2)}{y}} \quad \text{for } y \leq 1. \quad (34)$$

and the lens parameters are not determined for $y \geq 1$. We note that even for $y = 3$ the lens parameters can be extracted for $M_{Lz} \sim 10^6 - 10^8 M_\odot$ due to the wave effects. For $y = 0.1$ and 0.3 , the asymptotic behavior of errors are somewhat smaller than the results in Eq.(34), because the order of $1/f$ term in $F(f)$ (which is neglected in the geometrical optics approximation $f \rightarrow \infty$) affects the results. For $y = 1$, the errors decrease as lens mass increases as shown in Fig.9, because the errors converge to the results in the geometrical optics limit of Eq.(34) which vanish at $y = 1$. As a result, if $y > 1$, the errors asymptotically increase with the increase of the lens mass, but if $y < 1$, they asymptotically converge to constants.

Fig.10 is the same as Fig.9, but as a function of y . We note that even for larger $y \gtrsim 1$ we can extract the lens information. Thus the lensing probability ($\propto y^2$) to determine the lens parameters increases as compared with the results in geometrical optics limit for the lens objects in the mass range $10^6 - 10^8 M_\odot$.

4.3. Lensing Effects on the Estimation Errors of the Binary Parameters

We discuss the gravitational lensing effects on the estimation errors of the SMBH binary parameters. We study five binary parameters; the redshifted chirp mass \mathcal{M}_{cz} , the reduced mass μ_z , the distance to the source D_S and the angular resolution $(\bar{\theta}_S, \bar{\phi}_S)$. We find that the estimation errors of these parameters decrease because S/N increases by lensing (see Fig.5 and 6). The error $\Delta\gamma$ is roughly proportional to the inverse of the S/N as $\Delta\gamma \propto (S/N)^{-1}$ (see Eq.(30) and (31)).

4.4. Results for Various SMBH Masses and Redshifts

So far we presented the results for equal mass SMBH binaries with redshift $z_S = 1$. In this section, we comment the results for the case of various (unequal) SMBH masses $10^4 - 10^7 M_\odot$ and redshifts $z_S = 1 - 10$.

The critical lens mass in which the wave effects become important ($10^6 - 10^8 M_\odot$) is

mainly determined by the inverse of the knee frequency of the LISA’s noise spectrum, $\sim 8 \times 10^6 M_\odot (f/\text{mHz})^{-1}$, independent of the binary mass (see section 4.1). But for the massive total mass binary ($M_{1z} + M_{2z}$) $\gtrsim 10^7 M_\odot$, the binary coalescences at the lower frequency ($\sim 10^{-4}\text{Hz}$), thus the critical lens mass is shifted for larger mass ($10^7 - 10^9 M_\odot$). For the larger lens mass $M_{Lz} \gtrsim 10^8 M_\odot$, the results (the S/N increase and the estimation errors) converge to that in the geometrical optics limit irrespective of the binary mass. The estimation errors in Fig.7-10 are the case of $10^6 - 10^6 M_\odot$ binary at redshift $z_S = 1$ and are normalized to $S/N = 10^3$ and simply scale as $(S/N)^{-1}$. In order to translate the results in the various unequal SMBH binaries, we present the S/N for binary masses $M_{1,2z} = 10^4 - 10^7 M_\odot$ with redshifts $z_S = 1, 3, 5, 10$ in Table.1. We assume 1 yr observation of in-spiral phase before final merging. The results are the mean value of 100 binaries which are randomly distributed at each redshift, and the dispersion is relatively large $\sim 50\%$. From Table.1, one could translate the results in Fig.7-10 into errors in real situations.

We also comment the results for the case of only h_I data available, while we used the combination of h_I and h_{II} data (see section 3.1). In this case, the S/N increase in Fig.5 and 6 are not changed, but the estimation errors are slightly larger ($\sim 30\%$) than that in Fig.7-9 for $M_{Lz} \lesssim 10^7 M_\odot$ if the errors are normalized to $S/N = 10^3$. We note that the S/N is $\sqrt{2}$ times smaller than that in the case of the two data available in Table.1.

5. Lensing Event Rate

We discuss the event rate of merging SMBHs and estimate the lensing probability and the lensing event rate. The expected rate of merging SMBHs detected by LISA is in the range $0.1 - 10^2$ events per year (Haehnel 1994,1998). Recently, Wyithe & Loeb (2002) suggested that some hundreds detectable events per year could be expected, considering the merger rate at exceedingly high redshift ($z > 5 - 10$). Thus we take ~ 300 events per year as the merging event rate.

We consider the lens objects distributed over the universe and calculate the lensing probability for each lens model. For the point mass lens, we take the compact objects ($10^6 - 10^9 M_\odot$) such as black holes as lens. Denoting the mass density parameter of compact objects as Ω_{CO} , the lensing probability for a source at redshift z_S is (Schneider, Ehlers & Falco 1992),

$$P(z_S) = \frac{3}{2} \Omega_{\text{CO}} y_{cr}^2 \int_0^{z_S} dz_L \frac{(1+z_L)^2}{H(z_L)/H_0} \frac{H_0 D_{LS}(z_L, z_S)}{H_0 D_S(z_S)} \frac{H_0 D_L(z_L)}{H_0 D_S(z_S)}, \quad (35)$$

where $H(z)$ is the Hubble parameter at redshift z . The cosmological abundance of the compact objects in the mass range $10^6 - 10^9 M_\odot$ is limited by $\Omega_{\text{CO}} \leq 0.01$ by the search for

multiple images in radio sources (Wilkinson *et al.* 2001; see also Nemiroff *et al.* 2001). In Table 2, we show the upper limit on the lensing probability for the point mass lens. Since we set $y_{cr} = 10$ (Eq.(33)), the lensing probability is one hundred times larger than that normally assumed for the strong lensing of light ($y_{cr} = 1$). As shown in Table 2, the upper limit of the lensing probability is very high (almost 1) and is typically $\sim (\Omega_{CO}/10^{-2})$. The lensing event rate is the product of the merging rate (~ 300 per year) and the lensing probability, so that the lensing events will be 1 event per year if $\Omega_{CO} = 10^{-4}$.

For the SIS model we take CDM halos ($10^6 - 10^9 M_\odot$) as the lens objects (e.g. Narayan & White 1988). The lensing probability is

$$P(z_S) = \pi y_{cr}^2 \int_0^{z_S} dz_L \frac{(1+z_L)^2}{H(z_L)/H_0} \frac{H_0 D_{LS}(z_L, z_S)}{H_0 D_S(z_S)} \frac{H_0 D_L(z_L)}{H_0 D_S(z_S)} \int_{10^6 M_\odot}^{10^9 M_\odot} dM_L v N_v(v, z_L), \quad (36)$$

where N_v is the comoving number density of the lens and is assumed to be given by the Press-Schechter velocity function (Press & Schechter 1974) with $\sigma_8 = 1$. In Table 2, we show the lensing probability for the SIS model. We set $y_{cr} = 3$ (see Fig.9) and hence the lensing probability is almost ten times larger than that for light ($y_{cr} = 1$). As shown in Table 2, the lensing probability is typically $\sim 10^{-4} - 10^{-3}$. The merger rate is ~ 300 events per year at high redshift ($z > 5$), then the lensing events would be 1 event per year.

We note that the results in Table.2 are for the case of the $S/N = 10^3$, and are somewhat overestimated for the binaries of $S/N < 10^3$ in Table.1. For example, the lensing probability is proportional to (S/N) from Eq.(33) for the point mass lens, and it is appropriate to use $y_{cr} = 1$ for $S/N < 10^3$ in the SIS. In the case of the high event rate (~ 300 events/year), many fainter signals ($S/N \ll 10^3$) are expected and we note that the errors in Fig.7-10 are worse for these binaries.

Next, we discuss how we can identify the lensing signal. If the lensing event occurs, the amplitude and the arrival time of the gravitational waves are changed by lensing. But the other features (such as binary mass) are not changed. Thus, if the two signals have the same binary parameters (such as chirp mass) except for the amplitude and the arrival time, that would be a signature of gravitational lensing in the geometrical optics limit. More generally, oscillatory behavior in the waveform $|\tilde{h}^L(f)|$ is a signature of gravitational lensing (see Fig.4). However it will be difficult to identify the source and the lens objects in the sky, since the angular resolution of the LISA is ~ 1 deg (see Cutler 1998). Furthermore, the gravitational wave amplitude is changed by the lensing magnification and hence one must assume the lens model in order to determine the distance to the source. (Effect of lensing on measuring the distance is recently discussed in Holz & Hughes (2002).) As one determines the distance to the source $D_S(z_S)$, the redshift $z_S(D_S)$ could be determined if the cosmological parameters are well known (see Hughes 2002).

6. Summary

We have discussed the gravitational lensing of gravitational waves from chirping binaries, taking account of the wave effects in gravitational lensing. The SMBH binary is taken as the source detected by LISA, and the two simple lens models are considered: the point mass lens and the SIS model. We calculate the lensing effects on the signal to noise ratio (S/N) and how accurately the information of the lens object, its mass, can be extracted from the lensed signal. As expected, for the lens mass smaller than $10^8 M_\odot$, the wave effects are very important to calculate the S/N and the errors in the estimation parameters. It is found for the lens mass smaller than $10^6 M_\odot$ the signals are not magnified by lensing due to the diffraction effect. For the lens mass larger than $10^8 M_\odot$ the lens parameters can be determined within (very roughly) $\sim 0.1\% [(S/N)/10^3]^{-1}$. We note that the lensing cross section to determine the lens parameters is order of magnitude larger than that for light.

In this paper, we calculate the case for LISA. But similar analysis can be done for other detectors. For the ground-based interferometers (TAMA300, LIGO, VIRGO, GEO600), neutron star binaries are taken as the sources and the lens mass for which the wave effects become important is $10 - 10^4 M_\odot$. Similarly for the space-based interferometers such as DECIGO (Seto, Kawamura & Nakamura 2001), the important lens mass becomes $10^5 - 10^7 M_\odot$. Since mergers of neutron star binaries will be detected at least several per year for LIGO II (Phinney 1991; Kalogera *et al.* 2001) and $\sim 10^5$ per year for DECIGO, the lensing events would also be expected for other detectors.

We would like to thank Naoki Seto and Takeshi Chiba for useful comments and discussions. This work was supported in part by Grant-in-Aid for Scientific Research of the Japanese Ministry of Education, Culture, Sports, Science and Technology, No.14047212 (TN), and No.14204024 (TN).

A. Estimation errors in the geometrical optics limit

To evaluate the estimation errors $\Delta M_{Lz}, \Delta y$ in the geometrical optics limit, we consider the simple waveform;

$$\tilde{h}^L(f) = \left(|\mu_+|^{1/2} - i |\mu_-|^{1/2} e^{2\pi i f \Delta t_d} \right) \times \tilde{h}(f), \quad (\text{A1})$$

where $\tilde{h} \propto \mathcal{A}$ is the unlensed signal and $\Delta t_d \propto M_{Lz}$, with three parameters $\gamma_i = (\ln M_{Lz}, y, \ln \mathcal{A})$. Then, the Fisher matrix $\Gamma_{ij}(i, j = 1, 2, 3)$ in Eq.(30) can be analytically obtained as,

$$\Gamma_{11} = (2\pi \Delta t_d)^2 |\mu_-| (f \tilde{h} | f \tilde{h}),$$

$$\begin{aligned}
\Gamma_{12} &= 4\pi^2 \Delta t_d \frac{\partial \Delta t_d}{\partial y} |\mu_-| (f\tilde{h}|f\tilde{h}), \\
\Gamma_{13} &= 0, \\
\Gamma_{22} &= \frac{1}{4} \left[\frac{1}{|\mu_+|} \left(\frac{\partial |\mu_+|}{\partial y} \right)^2 + \frac{1}{|\mu_-|} \left(\frac{\partial |\mu_-|}{\partial y} \right)^2 \right] (\tilde{h}|\tilde{h}) + \left(2\pi \frac{\partial \Delta t_d}{\partial y} \right)^2 |\mu_-| (f\tilde{h}|f\tilde{h}), \\
\Gamma_{23} &= \frac{1}{2} \frac{\partial}{\partial y} (|\mu_+| + |\mu_-|) (\tilde{h}|\tilde{h}), \\
\Gamma_{33} &= (|\mu_+| + |\mu_-|) (\tilde{h}|\tilde{h}), \tag{A2}
\end{aligned}$$

and $\Gamma_{ji} = \Gamma_{ij}$. $(\tilde{h}|\tilde{h})$ and $(f\tilde{h}|f\tilde{h})$ in the above equation (A2) are,

$$\begin{aligned}
(\tilde{h}|\tilde{h}) &= (S/N)^2 = 4 \int \frac{df}{S_n(f)} \left| \tilde{h}(f) \right|^2, \\
(f\tilde{h}|f\tilde{h}) &= 4 \int \frac{df}{S_n(f)} \left| f\tilde{h}(f) \right|^2. \tag{A3}
\end{aligned}$$

The S/N is the signal to noise ratio for the unlensed signal \tilde{h} . The estimation errors can be analytically obtained by the inverse of the Fisher matrix, $\Delta M_{Lz}/M_{Lz} = [(\Gamma^{-1})_{11}]^{1/2}$ and $\Delta y/y = [(\Gamma^{-1})_{22}]^{1/2}/y$. Using the geometrical optics approximation, $f\Delta t_d \gg 1$, we obtain the errors with Eq.(A2) and (A3) as

$$\begin{aligned}
\frac{\Delta M_{Lz}}{M_{Lz}} &= \frac{1}{S/N} \times \sqrt{\frac{|\mu_+| + |\mu_-|}{|\mu_+ \mu_-|}} \left| 2 \frac{\partial}{\partial y} \ln \Delta t_d \Big/ \frac{\partial}{\partial y} \ln \left| \frac{\mu_+}{\mu_-} \right| \right|, \\
\frac{\Delta y}{y} &= \frac{1}{S/N} \times \sqrt{\frac{|\mu_+| + |\mu_-|}{|\mu_+ \mu_-|}} \left| 2 \Big/ y \frac{\partial}{\partial y} \ln \left| \frac{\mu_+}{\mu_-} \right| \right|. \tag{A4}
\end{aligned}$$

The above equations (A4) are used for the general lens model when the double images form.

REFERENCES

- Bender, P.L. *et al.*, LISA: A Cornerstone Mission for the Observation of Gravitational Waves, System and Technology Study Report ESA-SCI(2000) 11, 2000.
- Baraldo, C., Hosoya, A. & Nakamura, T.T., Phys. Rev. D, **59**, 083001, (1999).
- Bliokh, P.V. & Minakov, A.A., Ap. Space Sci., **34**, L7, (1975).
- Bontz, R.J. & Haugan, M.P., Ap. Space Sci., **78**, 199, (1981).
- Cutler, C. & Flanagan, E.F., Phys. Rev. D, **49**, 2658, (1994).

- Cutler, C., Phys. Rev. D, **57**, 7089, (1998).
- Cutler, C. & Thorne, K.S., gr-qc/0204090, (2002).
- Deguchi, S. & Watson, W.D., ApJ, **307**, 30, (1986).
- Deguchi, S. & Watson, W.D., Phys. Rev. D, **34**, 1708, (1986).
- De Paolis, F., *et al.*, Astron.Astrophys., **394**, 749, (2002).
- Finn, L.S., Phys. Rev. D, **46**, 5236, (1992).
- Haehnelt, M.G., MNRAS, **269**, 199, (1994).
- Haehnelt, M.G., in AIP Conf. Proc. 456, Second International LISA Symposium on the Detection and Observation of Gravitational Waves in Space, ed. W. M. Folkner (New York: AIP), 45, (1998).
- Hellings, R.W. & Moore, T.A., gr-qc/0207102, (2002).
- Holz, D.E. & Hughes, S.A., astro-ph/0212218, (2002).
- Hughes, S. A., MNRAS, **331**, 805, (2002).
- Kalogera, V., *et al.*, **556**, 340, (2001).
- Mandzhos, A.V., Soviet Astron. Lett., **7**, 213, (1981).
- Misner, C.W., Thorne, K.S. & Wheeler, J.A., Gravitation, (Freeman, San Francisco 1973).
- Moore, T.A. & Hellings, R.W., Phys. Rev. D **65**, 062001, (2002).
- Nakamura, T.T., Phys. Rev. Lett., **80**, 1138, (1998).
- Nakamura, T.T. & Deguchi, S., Prog. Theor. Phys. Suppl., **133**, 137, (1999).
- Narayan, R. & White, S.D.M., MNRAS, **231**, 97, (1988).
- Nemiroff, R.J., *et al.*, Phys. Rev. Lett., **86**, 580, (2001).
- Ohanian, H.C., Int. J. Theor. Phys., **9**, 425, (1974).
- Ohanian, H.C., ApJ, **271**, 551, (1983).
- Peters, P.C., Phys. Rev. D, **9**, 2207, (1974).
- Peterson, J.B. & Falk, T., ApJ, **374**, L5, (1991).

- Phinney, E.S., ApJ, **380**, L17, (1991).
- Press, W.H. & Schechter, P., ApJ, **187**, 425, (1974).
- Ruffa, A.A., ApJ, **517**, L31, (1999).
- Schneider, P. & Schmid-Burgk, J., A & A, **148**, 369, (1985).
- Schneider, P., Ehlers, J. & Falco, E.E., Gravitational Lenses, 1992, (New York : Springer).
- Seto, N., gr-qc/0210028, (2002).
- Seto, N., Kawamura, S. & Nakamura, T., Phys. Rev. Lett., **87**, 221103, (2001).
- Thorne, K.S., in *Gravitational Radiation*, edited by Deruelle, N. & Piran, T., (North-Holland, Amsterdam), p28, (1983).
- Turner, E.L., Ostriker, J.P. & Gott, J.R., ApJ, **284**, 1, (1984).
- Vecchio, A. & Cutler, C., in Folkner, W.M., editor, *Laser Interferometer Space Antenna, Second International LISA Symposium on the Detection and Observation of Gravitational Waves in Space*, AIP Conference Proceedings, Vol.456, p101, (1998).
- Vecchio, A., astro-ph/0304051, (2003).
- Wilkinson, P.N., *et al.*, Phys. Rev. Lett., **86**, 584, (2001).
- Wyithe, J.S.B. & Loeb, A., astro-ph/0211556, (2002).
- Zakharov, A.F. & Baryshev Yu,V., Class. Quant. Grav., **19**, 1361, (2002).

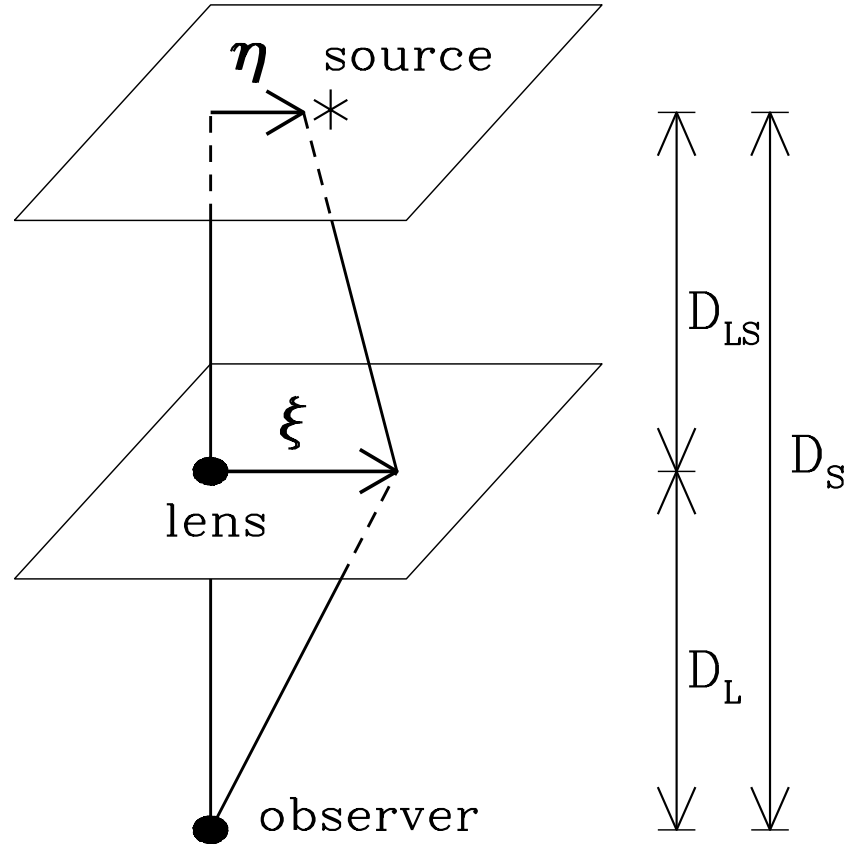


Fig. 1.— Gravitational lens geometry for the source, the lens and the observer. D_L, D_S and D_{LS} are the distances between them. η is a displacement of the source and ξ is an impact parameter. We use the thin lens approximation in which the gravitational waves are scattered in the thin lens plane.

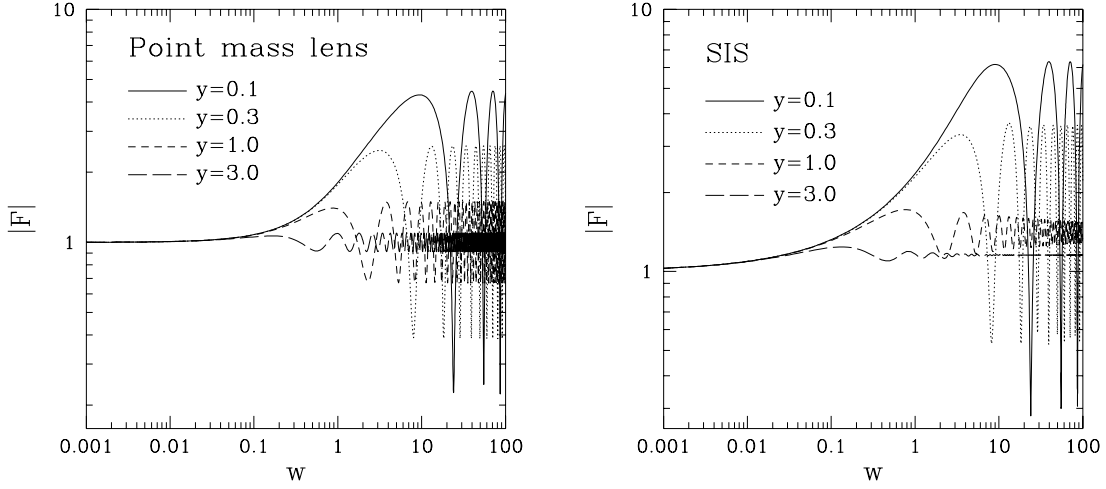


Fig. 2.— The amplification factor $|F(f)|$ as a function of $w (= 8\pi M_{Lz} f)$ with the fixed source position $y = 0.1, 0.3, 1, 3$ for the point mass lens (left panel) and the SIS (right panel). For $w \lesssim 1$, the amplification is very small due to the diffraction effect. For $w \gtrsim 1$, the oscillatory behavior appears due to the interference between the double images. We note for the SIS that even if $y \geq 1$ (a single image is formed in the geometrical optics limit) the damped oscillatory behavior appears.

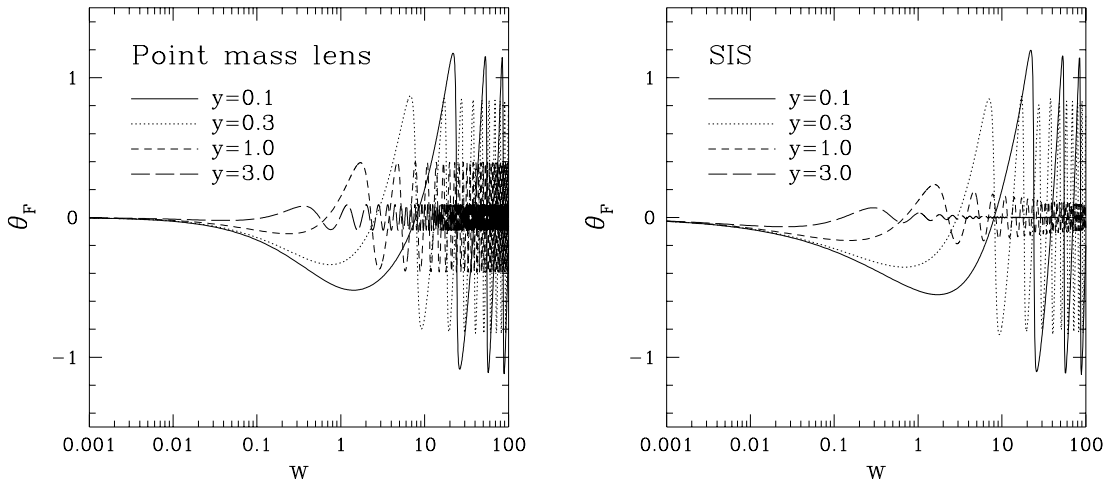


Fig. 3.— Same as Fig.2, but the phase of the amplification factor $\theta_F(f) = -i \ln[F(f)/|F(f)|]$ as a function of $w (= 8\pi M_{Lz} f)$.

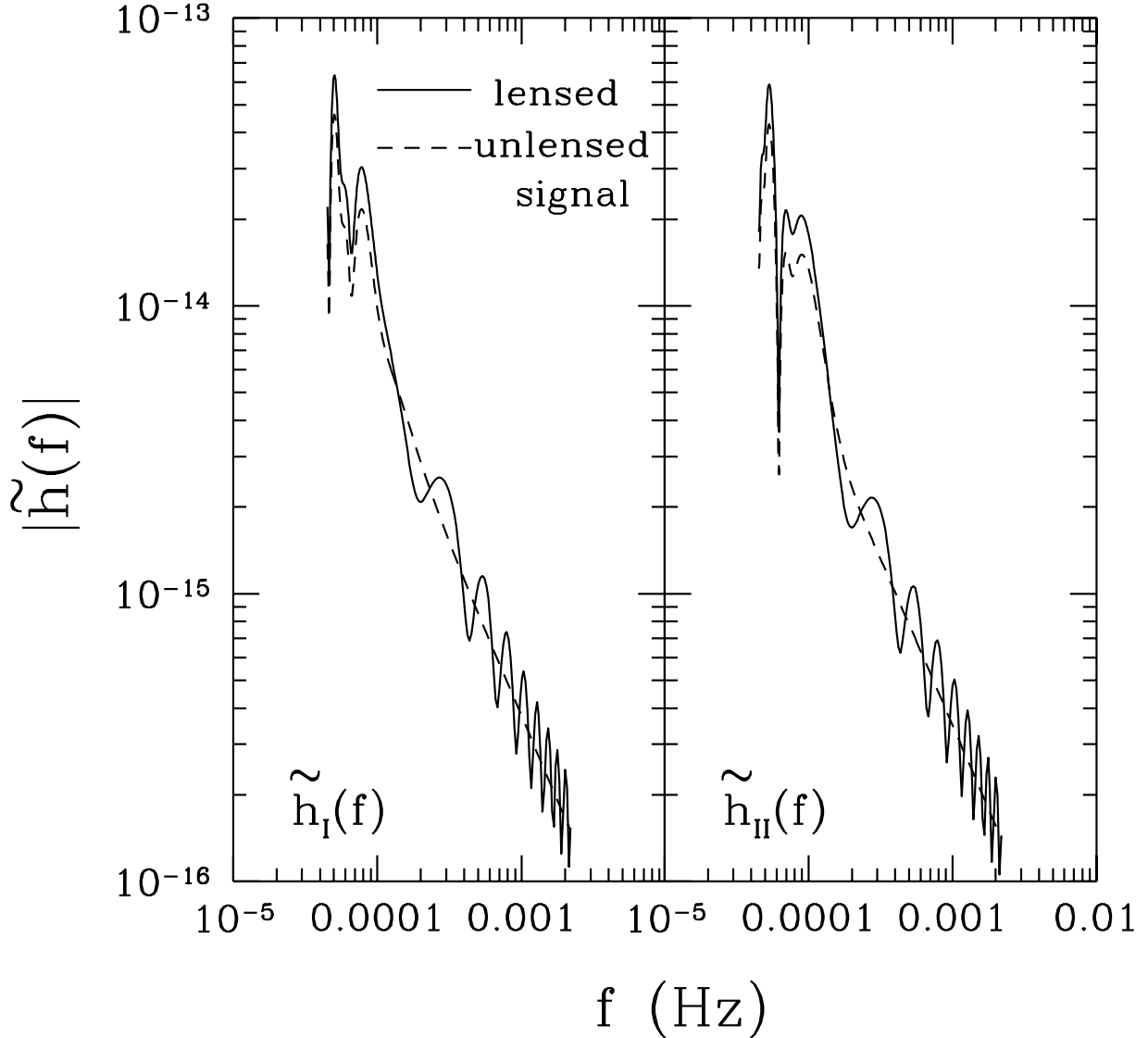


Fig. 4.— The lensed signals $|\tilde{h}_\alpha^L(f)|$ ($\alpha = I, II$) (solid line) and unlensed ones $|\tilde{h}_\alpha(f)|$ (dashed line) measured by LISA. The signals are shown from 1yr before coalescence to ISCO of $r = 6(M_1 + M_2)$. The redshifted masses of the SMBH binary is $M_{1,2z} = 10^6 M_\odot$, the redshifted lens mass is $M_{Lz} = 10^8 M_\odot$ and the source position $y = 1$. The angular parameters are $\cos \bar{\theta}_S = 0.3, \bar{\phi}_S = 5.0, \cos \bar{\theta}_L = 0.8, \bar{\phi}_L = 2.0$, and the source redshift is $z_S = 1$ (distance is $H_0 D_S = 0.386$). The strange behavior for $f \lesssim 10^{-4}$ Hz is due to the LISA orbital motion, and the difference between the two signals is small due to the diffraction. On the other hand, the oscillatory behavior appears for $f \gtrsim 10^{-4}$ Hz which is determined by the inverse of the lens mass $8\pi M_{Lz}$ (see Fig.2). This oscillation is due to the interference between the double images.

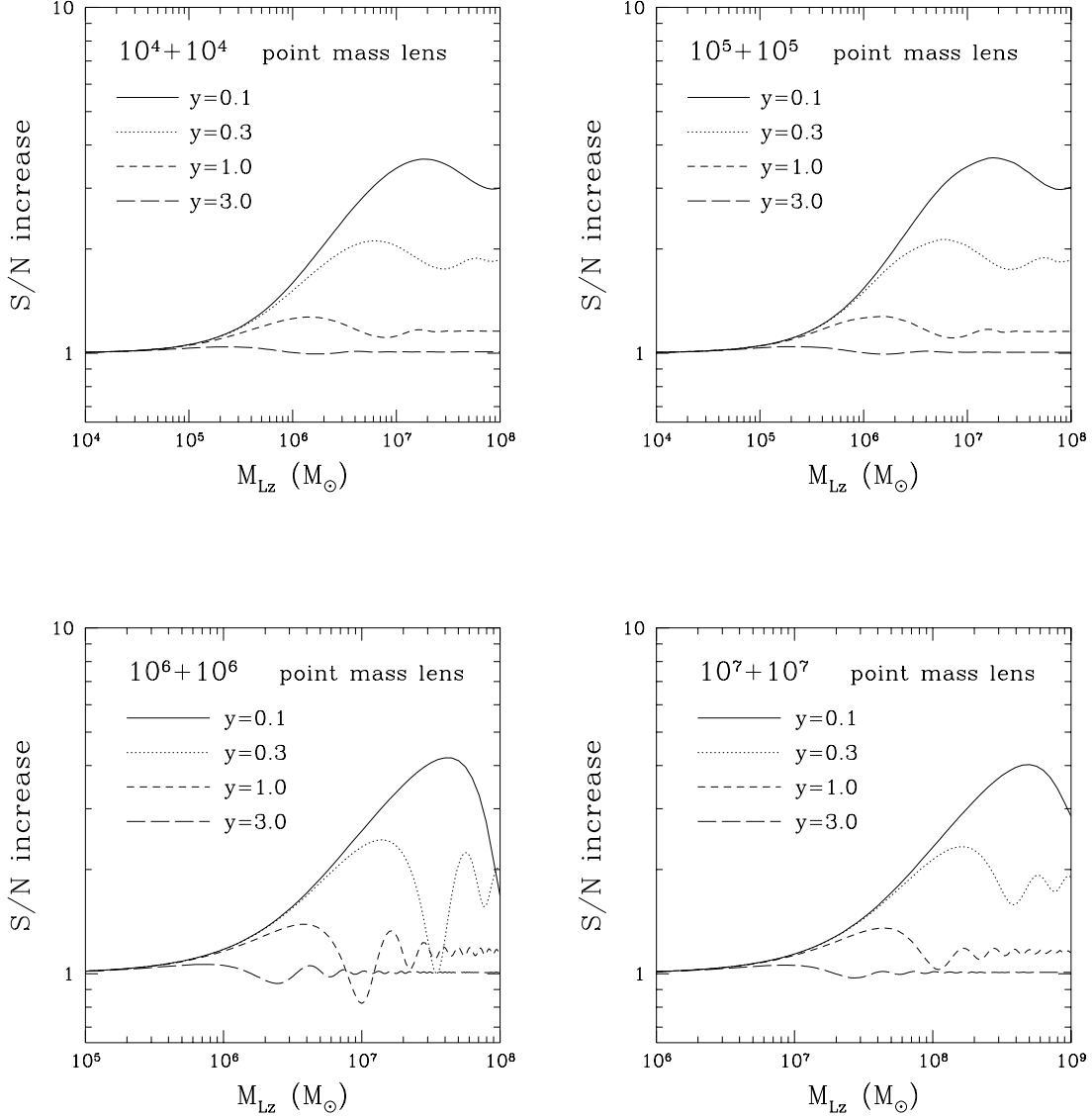


Fig. 5.— The increasing factor in S/N due to the gravitational lensing by the point mass lens for the various SMBH binary masses $M_{1,2z} = 10^4, 10^5, 10^6, 10^7 M_{\odot}$. The horizontal axis is the redshifted lens mass; the vertical axis is the lensed S/N divided by the unlensed S/N . The source position is fixed at $y = 0.1, 0.3, 1, 3$. For $M_{Lz} \lesssim 10^6 M_{\odot}$, the magnification is very small due to the diffraction effect irrespective of the SMBH binary masses. For $M_{Lz} \gtrsim 10^7 M_{\odot}$, the damped oscillatory patterns appear due to the interference between the two images, and this behavior converge in the geometrical optics limit, $|\mu|^{1/2} = (y^2 + 2)^{1/2} / [y^{1/2}(y^2 + 4)^{1/4}]$.

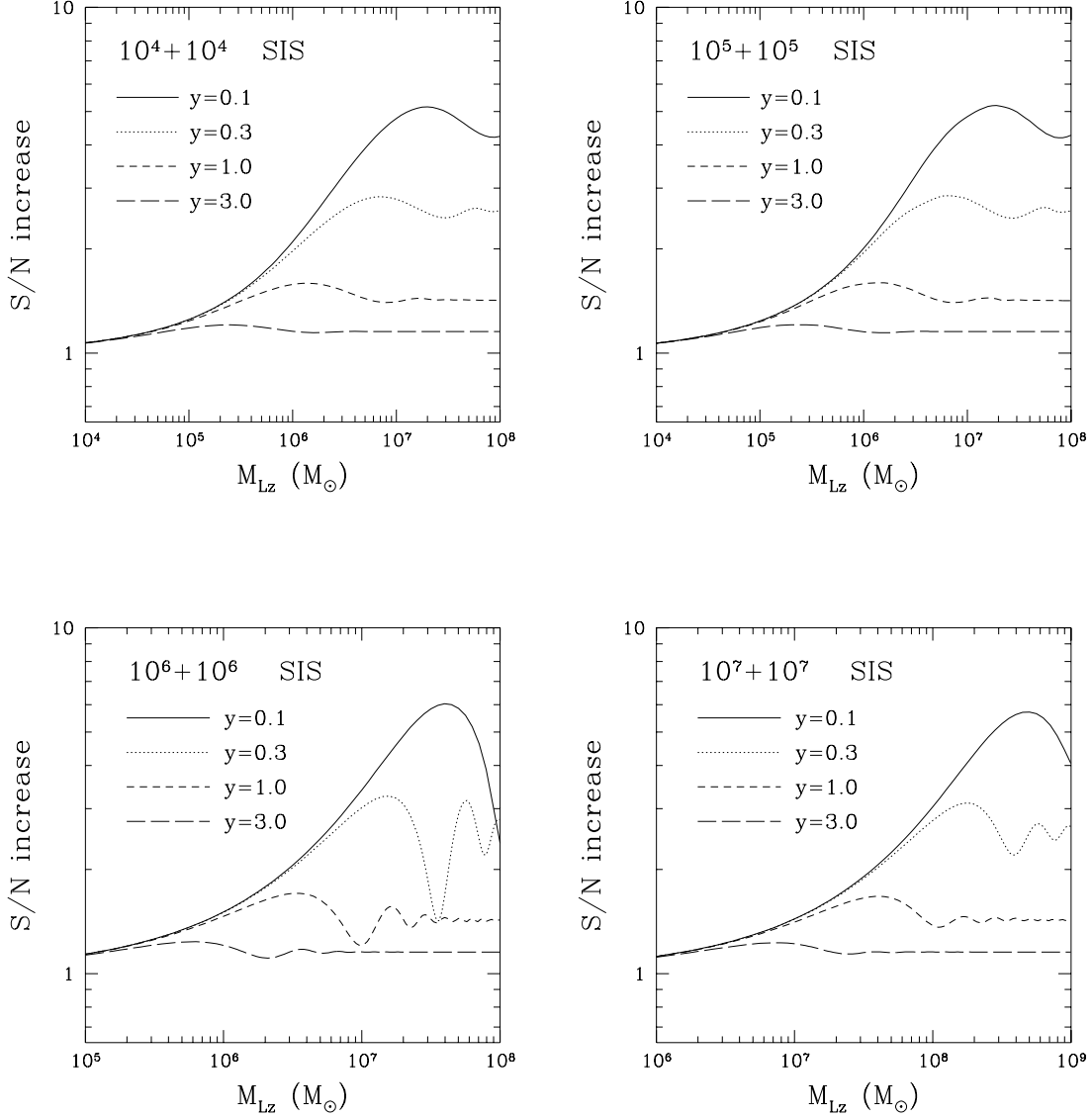


Fig. 6.— Same as Fig.5, but for the SIS lens model. For $M_{Lz} \gtrsim 10^7 M_\odot$, the results converge in the geometrical optics limit, $|\mu|^{1/2} = (2/y)^{1/2}$ for $y \leq 1$ and $|\mu|^{1/2} = (1 + 1/y)^{1/2}$ for $y \geq 1$.

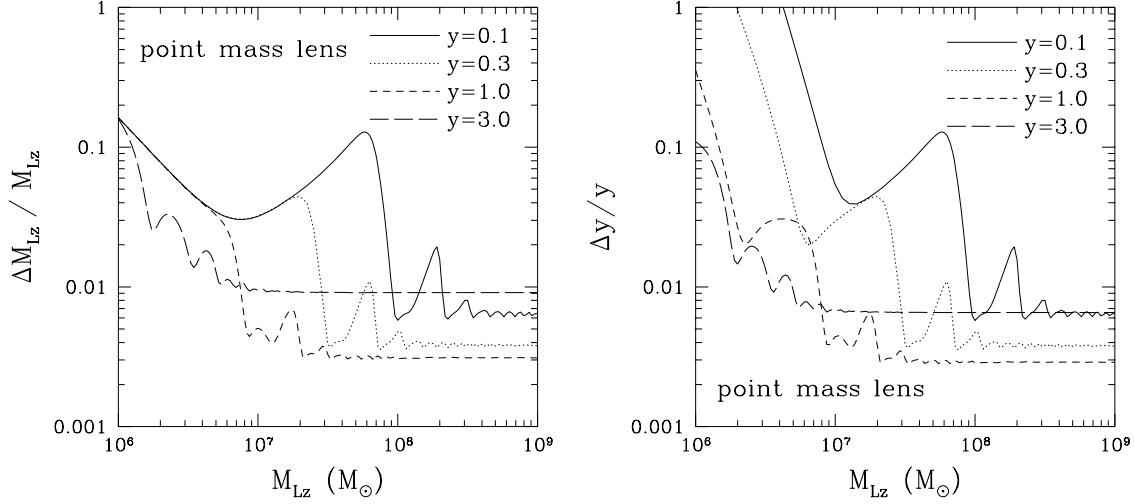


Fig. 7.— The estimation errors for the redshifted lens mass ΔM_{Lz} (left panel) and the source position Δy (right panel) for the point mass lens. The results are presented for the SMBH binary of masses $10^6 + 10^6 M_\odot$ at $z_S = 1$. The errors are normalized by $S/N = 10^3$ and simply scale as $(S/N)^{-1}$. For $M_{Lz} \lesssim 10^7 M_\odot$ the errors are relatively large, since the effect of lensing is very small due to the diffraction. For $M_{Lz} \gtrsim 10^8 M_\odot$ the geometrical optics approximation is valid, and errors converge to constants.

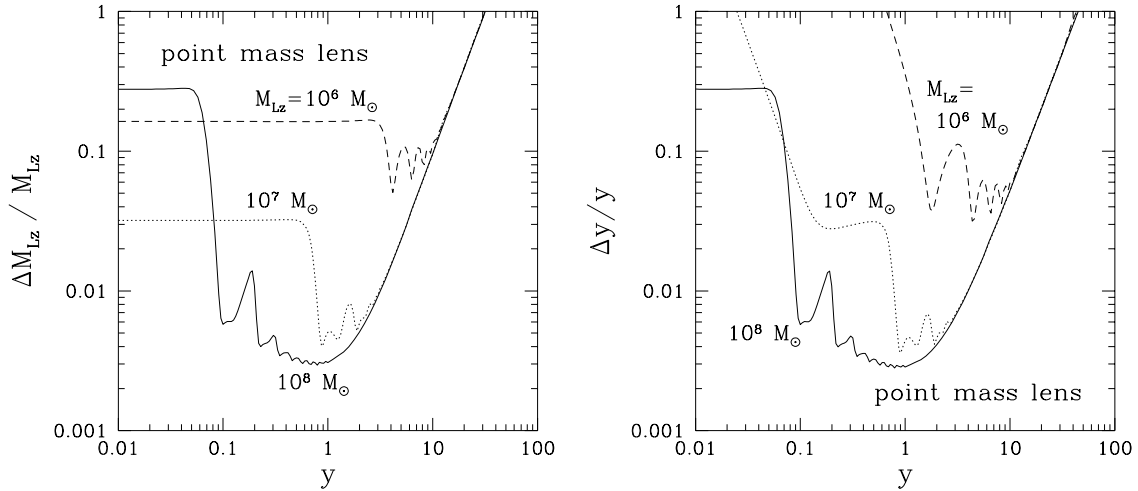


Fig. 8.— Same as Fig.7, but as a function of y . We note that even for $y \gtrsim 10$ we can extract the lens information. Then the lensing cross section ($\propto y^2$) increases an order of magnitude larger than that for the usual strong lensing of light ($y = 1$).

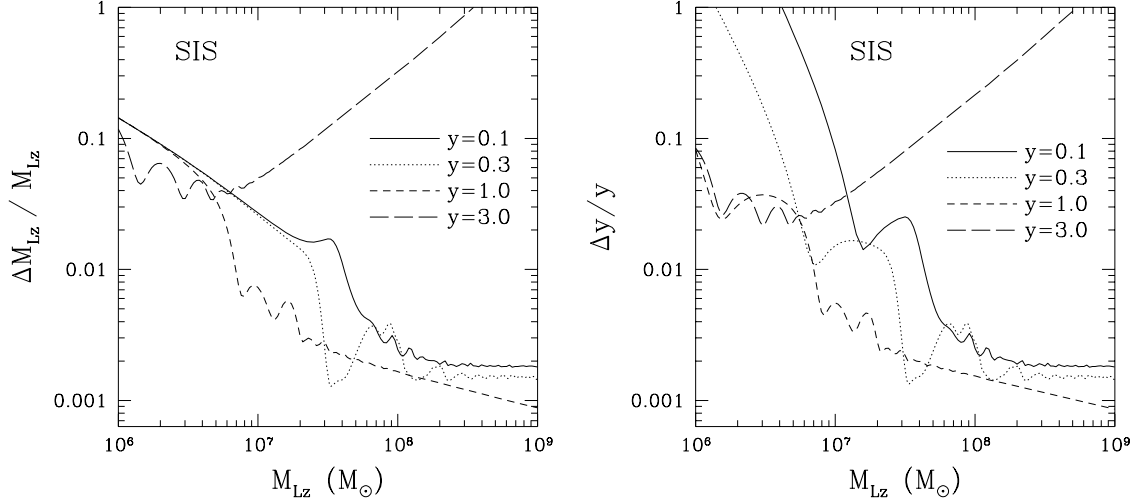


Fig. 9.— The estimation errors for the redshifted lens mass ΔM_{Lz} (left) and the source position Δy (right) for the SIS model. The results are presented for the SMBH binary of masses $10^6 + 10^6 M_\odot$ at $z_S = 1$. The errors are normalized by $S/N = 10^3$ and simply scale as $(S/N)^{-1}$. Even for $y = 3$ (a single image is formed in the geometrical optics limit), the lens parameters can be extracted at $M_{Lz} \sim 10^6 - 10^8 M_\odot$ due to the wave effects.

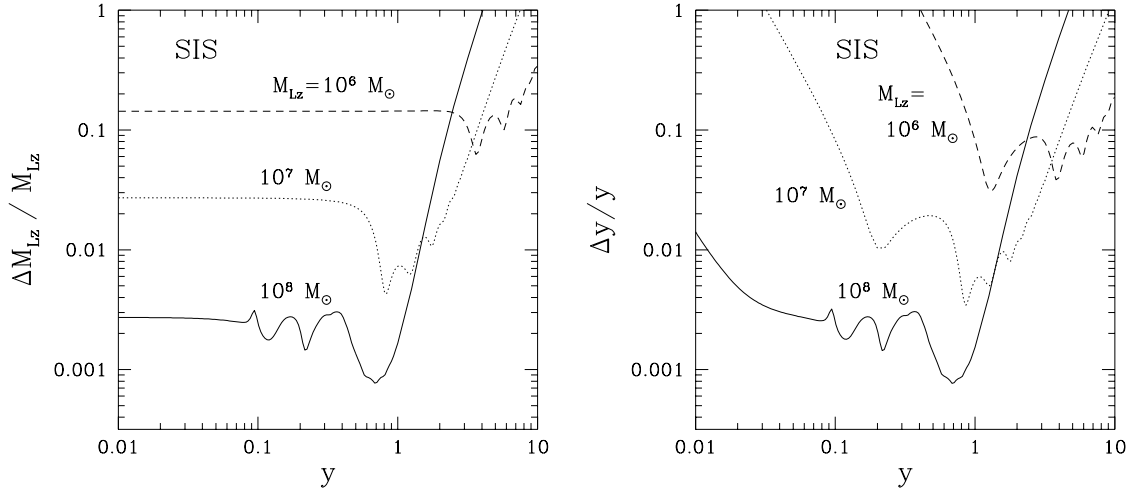


Fig. 10.— Same as Fig.9, but as a function of y . We note that even for $y > 1$ we can determine the lens parameters. Then the lensing cross section ($\propto y^2$) becomes larger than that in the geometrical optics approximation ($y = 1$).

Binary Masses (M_\odot)	$z_S = 1$	$z_S = 3$	$z_S = 5$	$z_S = 10$
$10^7 + 10^7$	1038	270	147	66
$10^7 + 10^6$	519	135	74	33
$10^7 + 10^5$	175	46	25	11
$10^7 + 10^4$	52	14	7	3
$10^6 + 10^6$	2575	669	365	164
$10^6 + 10^5$	1517	394	215	97
$10^6 + 10^4$	508	132	72	32
$10^5 + 10^5$	877	228	124	56
$10^5 + 10^4$	310	81	44	20
$10^4 + 10^4$	132	34	19	8

Table 1: The signal to noise ratio (S/N) for the various binary masses $10^4 - 10^7 M_\odot$ with redshift $z_S = 1, 3, 5, 10$. We assume 1 yr observation of in-spiral phase before final merging.

Lens Model	$z_S = 1$	$z_S = 3$	$z_S = 5$	$z_S = 10$
Point mass lens	< 0.21	< 1.1	< 2.0	< 3.9
SIS	7.2×10^{-5}	8.1×10^{-4}	2.0×10^{-3}	4.7×10^{-3}

Table 2: The lensing probability by the lens mass in the range $10^6 - 10^9 M_\odot$ with the source redshift $z_S = 1, 3, 5, 10$. For the point mass lens, we give the upper limit which is determined by the observational constraint on the abundance of the compact objects. When the lensing probability is more than one, the lensing occurs some times. For the SIS, CDM halos are assumed to be lenses. The presented values are for the case of $S/N = 10^3$, and hence the results are somewhat overestimated for the binaries of $S/N < 10^3$ in Table.1. If the expected rate of merging SMBHs is ~ 300 per year (Wyithe & Loeb 2002), then the lensing events will be detected 1 event per year.